

pubs.acs.org/crystal Article

Light-Triggered Rolling and Unrolling of Molecular Crystal Microsheets

Published as part of Crystal Growth & Design special issue "Celebrating Mike Ward's Contributions to Molecular Crystal Growth".

Pranaya P. Ghate, Cody J. Perry, Veronica Carta, Ibraheem Bushnak, Yahya J. Almuallem, Gregory J. O. Beran, Christopher J. Bardeen,* and Rabih O. Al-Kaysi*



Cite This: *Cryst. Growth Des.* 2024, 24, 7695–7703



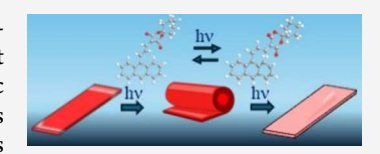
ACCESS

III Metrics & More



s) Supporting Information

ABSTRACT: The anthracene derivative (E)-3-(3-(anthracen-9-yl)allylidene)-1,5-dioxaspiro-[5.5]undecane-2,4-dione (E-ADUD) undergoes an $E \to Z$ photoisomerization in solution but not in crystals prepared by standard methods like solvent diffusion. However, the lipophilic cyclohexyl group facilitates precipitation of crystalline microsheets with submicron thicknesses from an aqueous solution containing sodium dodecyl sulfate and 1-dodecanol. These microsheets have horizontal dimensions on the order of 200 μ m and are composed of a metastable crystal



polymorph that permits the $E \to Z$ isomerization to proceed. Photoisomerization using visible light caused these microsheets to rapidly roll up into multilayer microcylinders with diameters ranging from 20 to 40 μ m. If the light was removed at this point, then the microscrolls were stable indefinitely. Continued exposure to visible light uncurled these cylindrical structures, reversing the mechanical process but not the photochemical reaction. The unrolled microsheets retained their crystallinity and could bend and twist under alternating UV and visible light but could not be rolled up again. The initial high curvature rolling up can be attributed to the creation of a surface layer of the Z-isomer that interacts with the underlying E-isomer crystal layer to generate a bimorph structure. Prolonged irradiation distributes the photoproduct more uniformly throughout the crystal and relieves this interfacial stress. The photoinduced rolling and unrolling could prove useful for applications like antenna or stent opening in hard-to-reach environments.

INTRODUCTION

When photoreactive molecules are organized within a crystal or polymer, their collective light-induced chemical reactions can be harnessed to generate motion on micro- or macroscopic length scales. 1-3 This photomechanical effect, where the molecules directly convert photon energy into mechanical work, has potential applications in light-activated artificial muscles and microrobots.⁴ Molecular crystals are the simplest chemical systems that can generate a photomechanical response, and their properties have become a subject of extensive study over the last two decades. 5,6 They have the advantage that precise structural information can be obtained through X-ray or electron diffraction methods, providing a way to connect molecular scale reaction dynamics to larger scale expansions and contractions. To enable a photomechanical response, the photoreactive molecules must first pack in such a way that they are able to photoisomerize or photodimerize. For example, it is possible for the same photochromic molecule to be either photomechanically active or inactive in the solid-state, depending on the crystal polymorph that is formed.^{7–9}

Beyond molecular packing, crystal size and shape also play a vital role in extracting efficient mechanical response from photomechanical crystals. In most cases, photomechanical crystals are studied in the form of flat microplates or long acicular crystals grown using standard methods such as sublimation or solvent diffusion. ^{10–17} But when the same molecule is processed under different conditions, it is possible to generate different crystal shapes (crystal habits) that lead to enhanced photomechanical performance. For example, large crystals made from 9-tert-butylanthracene ester shatter under UV light while nanowires with the same crystal packing, grown via solvent annealing inside anodic aluminum oxide (AAO) templates, expand uniformly along their long axis without breakage. ¹⁸

One "bottom-up" strategy to control photomechanical crystal properties is to identify growth conditions that favor a specific polymorphs and/or shapes. Ward and co-workers showed that nanoscale confinement provides one strategy, ^{19,20} while the use of different solvents and surfactants to control the growth rate and habit of molecular crystals has been demonstrated by multiple workers. ^{21–27} Our group has developed a general

Received: July 18, 2024 Revised: August 13, 2024 Accepted: August 16, 2024 Published: August 30, 2024





method to slowly precipitate photomechanical crystals via seeded growth in aqueous surfactants. We found that crystals grown using this method can exhibit different morphologies that enhance their photomechanical response. For example, bulk crystals of cis-dimethyl-2(3-(anthracen-9-yl)allylidene)malonate did not show any discernible photomechanical response, however microblock-like crystals, precipitated from an aqueous surfactant, could be peeled apart using pulses of UV light. Similarly long (Z)-2-(3-(anthracen-9-yl)allylidene)malononitrile microwires grown over several days from aqueous surfactant exhibit autonomous and continuous flagella-like motion under constant light irradiation, while larger bulk crystals with the same crystal packing displayed only a slight photomechanical response.²⁹ In both cases, the novel mechanical motions relied on E-Z photoisomerizations occurring in the crystal that generated internal stress. Given these findings, we were motivated to investigate the behavior of other molecules that had similar structures and could be crystallized using the surfactant growth method, with the goal of observing novel response modes powered by reversible $E \rightarrow Z$ photoisomerizations.

In this paper, we report the use of an aqueous suspension growth method to generate a novel photomechanical response from molecular crystals composed of (*E*)-3-(3-(anthracen-9-yl)allylidene)-1,5-dioxaspiro[5.5]undecane-2,4-dione (*E*-ADUD). This molecule undergoes an $E \rightarrow Z$ photoisomerization (Scheme 1) in solution but is inactive in crystals prepared

Scheme 1. Photoisomerization Reaction of *E*-ADUD to *Z*-ADUD under Visible Light^a

$$\begin{array}{c}
\lambda > 520 \text{ nm} \\
\hline
\lambda < 365 \text{ nm, or } \Delta T
\end{array}$$
E-ADUD
$$Z-ADUD$$

^aThe reverse reaction occurs under UV light irradiation.

using standard methods like solvent diffusion. This lack of response is due to a crystal polymorph that did not support the E → Z photoisomerization. Fortunately, the presence of a large lipophilic cyclohexyl group facilitates the precipitation of large microsheets from aqueous surfactant. Red colored monocrystalline microsheets of E-ADUD showed a remarkable photomechanical response when exposed to visible light. Upon visible light exposure they rolled up tightly in a fraction of a second and slowly unrolled back to their original flat shape with a noticeable fading of their red color. The unrolled microsheets retained their crystallinity and could bend and twist under alternating UV and visible light giving a P-type photomechanical crystal. We found that the microsheets were composed of a different, metastable polymorph that permits the $E \rightarrow Z$ isomerization to proceed while also facilitating the growth of ultrathin sheets that enable high curvature rolling. The rolled-up E-ADUD microsheets maintained their tightly rolled shape when the light is removed, making it possible to separate them from the aqueous suspension through filtration and image them using scanning electron microscopy. The E-ADUD system shows how a

combination of crystal engineering and shape control can generate crystals with a unique photomechanical response. This method of shaping crystals using light could find applications in biomedicine, where specially configured microcylinders could be programmed to unfurl on command.

EXPERIMENTAL SECTION

Synthesis. The synthesis and photoisomerization reaction of *E*-ADUD is outlined in the Supporting Information, Scheme S1. Additional details are provided in the Supporting Information. The synthesis of *E*-ADUD was performed under low light to minimize unwanted photoisomerization.

Growth of *E*-ADUD Microsheets. *E*-ADUD (10 mg, 2.5×10^{-5} moles) was dissolved in warm N,N-dimethylformamide (N,N-DMF, 0.5 mL) to obtain a 0.05 M concentration. An aqueous solution containing sodium dodecyl sulfate (SDS, 0.025 M) and 1-dodecanol (1-DD, 0.0025 M) was prepared and filtered at 40–50 $^{\circ}\text{C}$ through a 0.2- μ m nitrocellulose filter. This surfactant solution was maintained at 45 °C to prevent the SDS/1-DD cocrystals from precipitating. A 20 mL volume of the warm aqueous mixture was added to a clean 30 mL amber-colored vial and kept at 45 °C to reach thermal equilibrium. Then, 0.1 mL of the E-ADUD solution was injected into the warm surfactant solution, gently swirled, and placed in an oven at 35 °C for 10 min until the solution turned clear red. The vial containing the supersaturated E-ADUD solution in SDS/1-DD was tightly sealed and mounted on a Labquake tube rotator from Thermo Scientific, set at 8 rpm with the vial fixed parallel to the axes of rotation. The tube rotator was placed in a laboratory oven at 35 °C. Large microsheets of E-ADUD crystallized and remained suspended after 10-20 h. The crystalline microsheets were stable for months when filtered and stored at room temperature. If stored at 35 °C in the SDS/1-DD aqueous mixture, this unstable polymorph was gradually replaced by small orange crystal blocks characteristic of polymorph A after several days. When 0.5 mL of this microsheet suspension was injected into a freshly prepared vial of supersaturated E-ADUD in aqueous surfactant and placed undisturbed in an oven at 35 °C for a couple of hours, suspended microsheets with a more uniform size distribution were obtained.

Ultraviolet (UV)-Visible Spectroscopy. Absorption spectra of the samples were obtained using a Spectro UV—vis (UVD 2950) from Labomed Inc. with a 1 cm quartz cell (Starna Scientific) and a slit width of 1.0 nm. The scanning wavelength range selected was 200—700 nm. A solvent blank was collected before each measurement.

High-Performance Liquid Chromatography (HPLC). HPLC analysis was performed on a Shimadzu instrument (LC- 20AD) using a Thermo Scientific BDS Hypersil C18 column ($250 \times 4.6 \text{ mm}$) maintained at 308 K. A gradient mobile phase was used, starting with 50% acetonitrile in water (pH = 2.5) and ending with 100% acetonitrile at a flow rate of 1.0 or 1.5 mL/min. The detector wavelength was set to 254 nm

Nuclear Magnetic Resonance (NMR) Spectroscopy. 1 H NMR spectra were recorded on a JEOL (400 MHz) spectrometer at 298 K. 13 C NMR spectra were recorded on a JEOL (100 MHz) spectrometer with complete proton decoupling at 298 K. Proton chemical shifts were reported in ppm (δ) (DMSO- d_6 , δ 2.50 ppm) and J values were reported in hertz (Hz). Carbon chemical shifts were reported in ppm (δ) (DMSO- d_6 , δ 39.52 ppm). A 25% (V/V) mixture of DMSO- d_6 in CCl₄ was used instead of pure DMSO- d_6 to increase the solubility of the compound and prevent the solution from freezing.

Infrared (IR) Spectroscopy. IR spectroscopic measurements were performed on an IR Affinity-1 FTIR from Shimadzu. Approximately 1% of the sample was pulverized with spectroscopic grade KBr using an agate mortar and pestle and pressed into a transparent pellet.

Melting Points. Uncorrected melting points were measured using a 1101D Mel-Temp digital melting point apparatus.

Optical Microscopy. Microscopic imaging was performed using an upright fluorescence microscope from Optika, equipped with a 100 W medium-pressure Hg lamp and a 2 MP digital camera. Various excitation wavelengths were obtained through different optical filter combinations, with a typical irradiation intensity around 10 mW/cm².

Scanning Electron Microscopy (SEM). SEM measurements were performed using a JEOL JSM-6510LV scanning electron microscope. Samples were sputter-coated with a thin layer of Pt prior to imaging.

X-ray Diffraction. An orange crystal (block, approximate dimensions $0.09 \times 0.07 \times 0.05$ mm3) was placed onto the tip of a MiTeGen pin and mounted on a Bruker Venture D8 diffractometer equipped with a PhotonIII detector at 140.00 K. The data collection was carried out using Cu Ka radiation (l=1.54178 Å, ImS microsource) with a frame time of 2-10 s and a detector distance of 40 mm. A collection strategy was calculated and complete data to a resolution of 0.84 Å with a redundancy of 6.3 were collected. The frames were integrated with the Bruker SAINT software package (version 8.30A) using a narrow-frame algorithm to a resolution of 0.84 Å. Data were corrected for absorption effects using the Multi-Scan method (Bruker SADABS software package, version 2.03). Please refer to Table S1 for additional crystal and refinement information.

Structure Solution and Refinement for Polymorph A. The space group P-1 was determined based on intensity statistics and systematic absences. The structure was solved using the SHELX suite of programs 30,31 and refined using full-matrix least-squares on F^2 within the OLEX2 suite. 32 An intrinsic phasing solution was calculated, which provided most non-hydrogen atoms from the E-map. Full-matrix least-squares/difference Fourier cycles were performed, which located the remaining non-hydrogen atoms. All non-hydrogen atoms were refined with anisotropic displacement parameters. The hydrogen atoms were placed in ideal positions and refined as riding atoms with relative isotropic displacement parameters. The final full matrix least-squares refinement converged to R1 = 0.0476 and wR2 = 0.1349 (F^2 , all data). The goodness-of-fit was 1.058. On the basis of the final model, the calculated density was 1.348 g/cm³ and F(000), 420 e $^-$.

Electron Diffraction for Polymorph B. The Micro ED Core facility at the UCLA School of Medicine conducted Micro ED analyses of polymorph B samples. Electron-counted MicroED data was obtained using a Titan Krios 3 Gi TEM (Thermo Fisher) operated at 300 kV. Electron diffraction pattern tilt series data were recorded with a bottom mount TVIPS F416 4 k × 4 k CMOS camera with pixel size 15.6 m Susing built in series exposure mode. The electron dose was kept below 0.01 e-/Å² per second, and each frame of a data set was taken with an exposure time of up to 10 s per frame. The electron dosage was calibrated with the use of a Faraday cage as well as by calibrating the counts on the CMOS detector in bright field mode. Each data set consisted of up to 90 still frames taken at 0.1-1° intervals with a maximum total dose of 9 e⁻/Å² per crystal. The camera length was optimized for the desired resolution as described previously.³³ The structure was refined using the best combinations of data available. The structure came out very clearly from SHELXT using electron scattering factors.

Computational. Experimental crystal structures were optimized with plane-wave DFT in Quantum Espresso v6.5, 34 using the B86bPBE functional 35,36 under periodic boundary conditions. The exchange hole dipole moment (XDM) dispersion correction 37 was applied to treat noncovalent interactions more accurately. A 50 Ry plane-wave cutoff was used with a Monkhorst-Pack reciprocal space k-point grid density of at least 0.05 Å $^{-1}$. The core electrons were treated using the projector augmented wave (PAW) pseudopotential inside Quantum Espresso. To address the known limitations of generalizated gradient approximation functionals such as B86bPBE in describing the conformational energies of highly conjugated molecules, intramolecular conformational energies were computed with the revDSD-PBEP86-D4 double-hybrid density functional according to the procedures developed previously in our group. 38 The revDSD-PBEP86-D4 calculations were performed in Orca 5.0 39 using the def2-QZVP basis set

RESULTS AND DISCUSSION

The synthesis of *E*-ADUD was accomplished through a Knovenagel condensation between (*E*)-3-(anthracen-9-yl)-acrylaldehyde and 1,5-dioxaspiro[5.5]undecane-2,4-dione, an analog of Meldrum's acid (Supporting Information, Scheme

S1).⁴⁰ A similar derivative (E)-(5-(3-anthracen-9-yl-allylidene)-2,2-dimethyl-[1,3] dioxane-4,6-dione) (E-AYAD) was previously synthesized following the same synthetic methodology,⁴¹ and full details of the synthesis are given in the Supporting Information. The electron-withdrawing group on the divinyl tail, a Meldrum's acid analog, was chosen to shift the absorption spectrum of E-ADUD to longer wavelengths. The presence of a diolefin on the 9-carbon position of the anthracene enables the $E \rightarrow Z$ photoisomerization.

In solution, the absorption spectrum of *E*-ADUD is dominated by a broad, featureless peak at 460 nm with a tail that extends past 550 nm. When irradiated at 520 nm, the absorption spectrum evolved as shown in Figure 1, with a clear

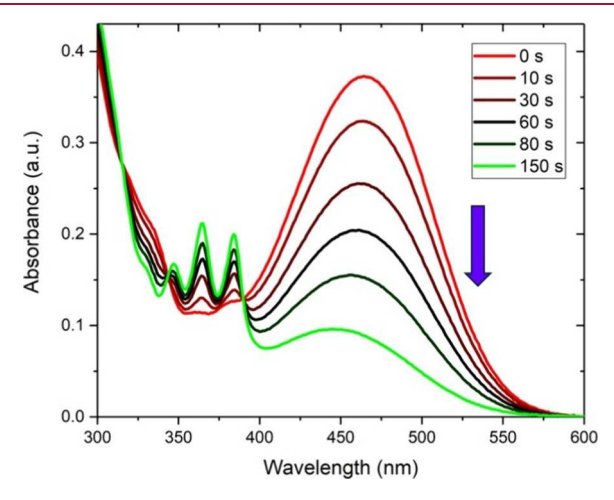


Figure 1. Absorption spectra of photoisomerization from *E*-ADUD (red) to Z-ADUD (green) in acetonitrile using light with a maximum wavelength centering at 520 nm. A clear isosbestic point at 390 nm is observed. The starting concentration of *E*-ADUD was 5.28×10^{-5} M.

isosbestic point at 390 nm. Using the 520 nm excitation wavelength from a commercial green LED, conversion to Z-ADUD in acetonitrile was about 94% as determined using HPLC analysis (Supporting Information, Figure S7a,b). The presence of overlapping bands between the E and Z isomers prevents complete photochemical conversion to the Z-ADUD. The Z-ADUD in acetonitrile can be partially converted back to the E-ADUD using UV light (365 nm), reaching a photostationary state composed of a 65:35 mixture of E:Z isomers as determined by HPLC (Supporting Information, Figure S7c). The Z-isomer has a half-life of ~24 h in acetonitrile at room temperature (293 K), as determined by HPLC analysis that measured the slow thermal conversion of Z-ADUD to E-ADUD in acetonitrile over a period of several days. (Supporting Information, Figure S8).

In the solid-state, E-ADUD exhibits two crystal polymorphs that have very different properties. Dark red crystals, grown by the slow diffusion of water vapor into a solution of E-ADUD in N,N-DMF, were photochemically stable when irradiated with visible or UV light. These block-like crystals had dimensions on the order of millimeters and were of high quality, so structure determination using standard X-ray diffraction techniques was straightforward. The packing in this polymorph, labeled as Polymorph A, showed a high density stacked arrangement in which the cyclohexyl tails of neighboring stacks interacted with each other, as shown in Figure 2a. Separated by 3.8 Å, the anthracene rings were close enough to support a $\begin{bmatrix} 4 + 4 \end{bmatrix}$ photodimerization. 42 Under visible light, crystals composed of

Crystal Growth & Design pubs.acs.org/crystal Article

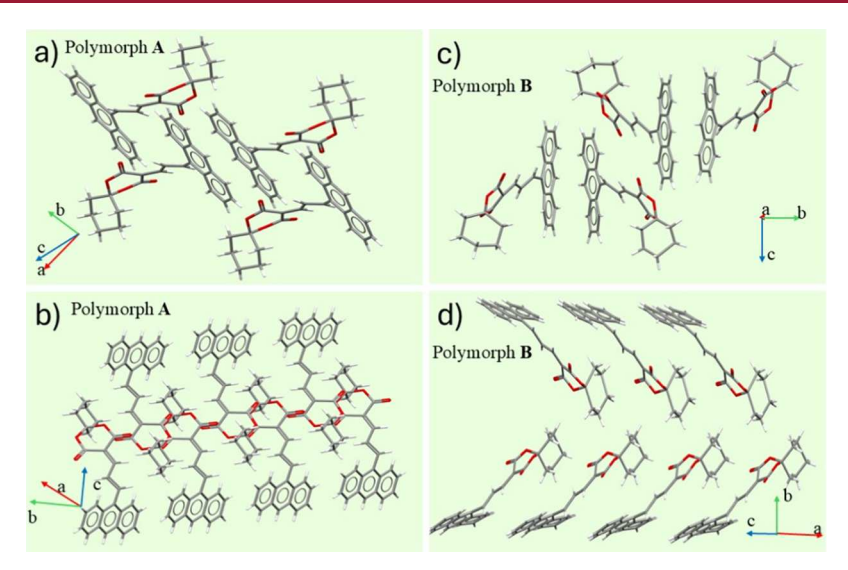


Figure 2. (a) Crystal packing of *E*-**ADUD** unreactive polymorph **A** showing anthracene pairs; (b) crystal packing polymorph **A** showing cyclohexyl ring corridor with interlocked side-chains; (c) crystal packing of reactive polymorph **B** showing anthracene pairing; (d) crystal packing of polymorph **B** showing cyclohexyl corridor with additional room for cyclohexyl side-chain motion.

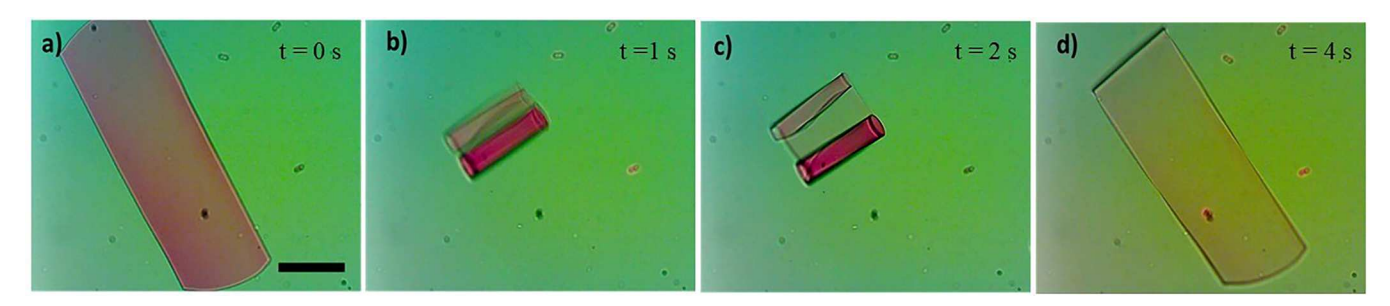


Figure 3. Optical microscope images of *E*-ADUD microsheet rolling and unrolling under continuous 520 nm light exposure. (a) Single crystal microsheet; (b) after 1 s of irradiation the sheet snap rolls into a tightly curled tube; (c) with continued irradiation, the microsheet starts to unroll slowly from both ends; (d) after 4 s the sheet returns to its original flat shape with a noticeable fading of color. Scale bar = 50 μ m.

polymorph **A** exhibited stable red fluorescence and showed no evidence of photoinduced changes like cracking, color change or bleaching. We suspect that the absence of [4+4] photodimerization may reflect the large size of the 9-position substituent, which has been shown to inhibit dimerization in other anthracene derivatives. 43 E \rightarrow Z isomerization is another possible pathway, but the congested cyclohexyl corridor leaves little room for rotation of the bulky tail required for this reaction.

In order to obtain a crystal packing that permitted the $E \rightarrow Z$ photoisomerization, we turned to the surfactant reprecipitation method described in the Introduction. When a solution of the E-ADUD in N,N-DMF was rapidly injected in an aqueous solution of SDS/1-DD at 45 °C, a clear red solution of the E-ADUD was formed. When subjected to gentle agitation using a tube rotator, this supersaturated solution slowly precipitated microsheets over a period of 10-20 h when incubated at 35 °C inside a laboratory oven. The microsheets were crystalline, showing high birefringence when observed using polarized light microscopy (Supporting Information, Figure S9). On average, the lengths of these microsheets were on the order of 500 μ m with widths of $100-200 \, \mu \text{m}$. The length and width values could vary by a factor of 2 within a sample, and the average dimensions varied depending on the growth conditions. By adding microcrystals of the polymorph B as seeds to a supersaturated solution of E-ADUD in an aqueous surfactant, more uniformly sized

microribbons could be formed at a faster rate at the cost of slightly reduced size.

The crystalline microsheets were too thin for structure determination using standard X-ray diffraction techniques. Fortunately, single crystal electron diffraction was successful in generating a crystal structure for polymorph B, which is shown in Figure 2b. In this polymorph, the anthracene rings were too far apart (4.5 Å) to support [4 + 4] photodimerization. Unlike polymorph A, the cyclohexyl tails were not interlocked in corridors between neighboring stacks but instead occupied cavities adjacent to the anthracene rings and each other. Presumably, this extra space for the cyclohexyl tails enabled the $E \rightarrow Z$ photoisomerization to proceed without largescale lattice disruption. We used periodic dispersion-corrected density functional theory to compute the relative energies of the two different polymorphs and found that polymorph A was 8.8 kJ/ mol more stable than polymorph B. It is an open question as to why surfactant growth favors polymorph B. It is well established that the use of surfactants can enable a molecule to crystallize into metastable crystal polymorphs. 44-47 The fact that **E-ADUD** adopts slightly different conformations in polymorphs A and B (Supporting Information, Figure S10) suggests that the surfactant may influence molecular conformation in solution to favor polymorph B packing.⁴⁸ Since polymorph control is vital for generating the photomechanical response, further investigation of this complex subject is clearly warranted.

Crystal Growth & Design pubs.acs.org/crystal Article

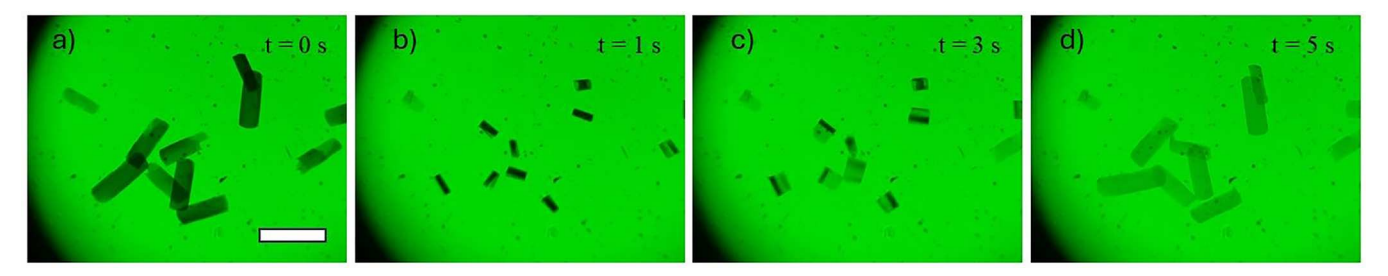


Figure 4. Population of *E*-ADUD crystalline microsheets rolling and unrolling simultaneously under continuous 520 nm irradiation. (a) Microsheets before irradiation; (b) rolled up microsheets at 1 s of light exposure; (c) with continued irradiation, the microsheets start unrolling simultaneously; (d) microsheets returned to their original flat shape in the next 2 s with a noticeable fading of color. Scale bar = $100 \mu m$.

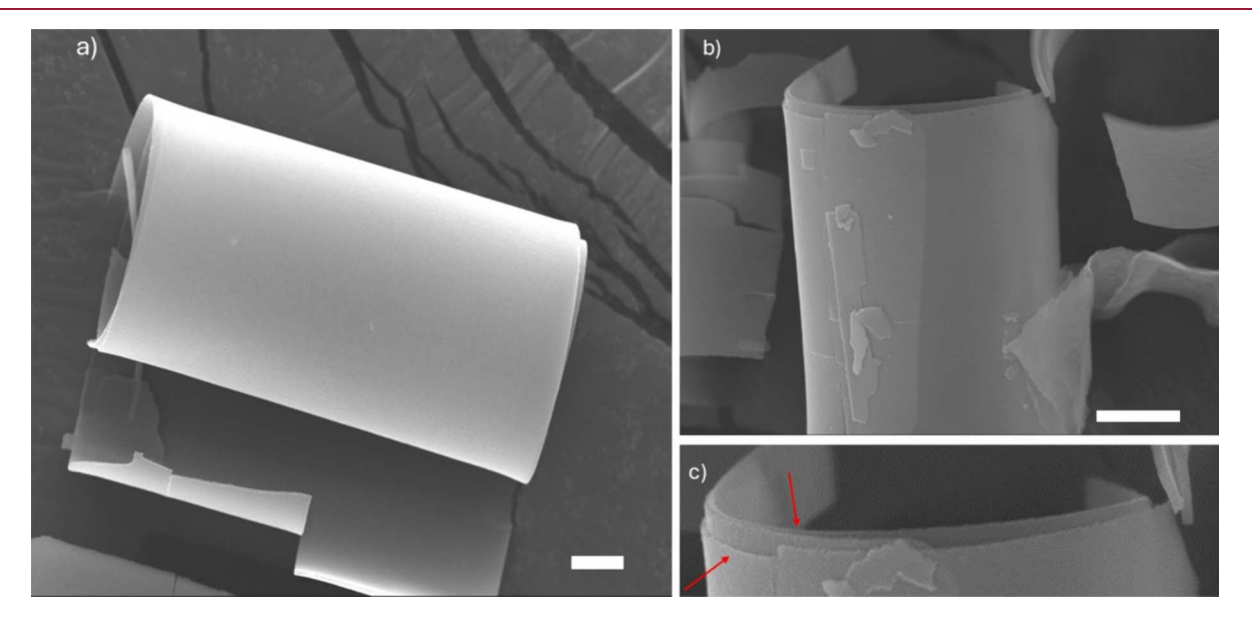
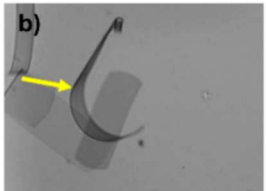


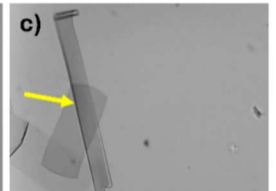
Figure 5. (a) Top-down SEM image of rolled-up *E*-ADUD crystal microsheet. The cracks appear after drying. (b) Side view of edge of a rolled-up microsheet showing layers formed during rolling. Other sheets can be seen in background. (c) Zoomed-in view of the top of the scroll in panel (b) showing nested crystal layers. Scale bars = $10 \mu m$.

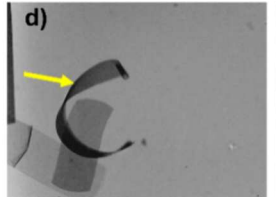
Although more challenging to grow, the metastable polymorph B was necessary to generate photomechanical motion. Microsheets deposited on a glass slide showed a typical photochemical response to visible light irradiation (520 nm) after washing away the surfactant and air-drying. In most cases, parallel cracks formed on the surface of the crystal with a few incidents of photosalient behavior (Supporting Information, Figure S11 and Movie S1). When the microsheets were left suspended in the aqueous growth solution, a more dramatic photomechanical response was observed. Exposure to wavelengths greater than 475 nm caused them to roll up into multiwalled cylinders with typical radii of 20-40 μ m (Figure 3a,b). Additional images and movies are given in Supporting Information, Figure S12 and Movie S2. Some thicker microsheets developed minor cracks while rolling when irradiated with visible light (Supporting Information, Movie S3), but nothing like the extensive cracking of the dry sheets. The lack of crack formation in the suspended microsheets might be due to their ability to freely deform in the absence of surface adhesion. An alternative explanation could be the Rehbinder effect, in which water and surfactant molecules reduce the stiffness of the crystal surface and prevent propagation of microscopic cracks formed during photodeformation. 49,50 To the best of our knowledge, the Rehbinder effect has not been studied in molecular crystals, but it is an intriguing possibility that could

explain the lack of cracking. Continued exposure of the rolled-up microsheets to visible light caused them to unroll without the formation of cracks (Figure 3c,d and Supporting Information, Movie S2). The sheets retained their birefringence after unrolling (Supporting Information, Figure S9b and Movie S4), indicating that the extreme curvature was due to a crystal-to-crystal photochemical reaction and not the formation of an amorphous phase by the E-Z photoisomerization. The behavior of the microsheets was remarkably uniform across a sample. A population of microsheets could roll up and unroll in unison when irradiated with visible light as seen in Figure 4. This behavior reflects the uniform thickness of the microsheets. Videos of this behavior can be found in the Supporting Information, Movies S5, S6, S7, S8, S9, and S10.

If the visible light was removed after the sheets rolled up, they retained their shape for at least 12 h in the suspension. We found that **Z-ADUD** was stable indefinitely in the solid-state, showing no signs of conversion back to the thermodynamically stable **E-ADUD** even after several months of room temperature storage. The stability of the rolled microsheets allowed them to be filtered from the solution and examined using SEM. When dried, the rolled microsheets occasionally formed longitudinal cracks. Close inspection of the rolled-up microsheets using SEM revealed a smooth curved crystal surface with several layers stacked on top of one another (Figure 5) with submicron sheet







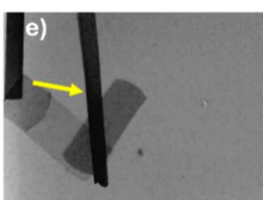


Figure 6. Optical microscope images of the photomechanical response of an *E*-**ADUD** microsheet after initial exposure to 520 nm has led to rolling up and unrolling. (a) Fully unrolled microsheet after exposure to 520 nm (duration 20 s), (b) exposure to 365 nm (duration 10 s) causes the sheet to bend but not roll up; (c) subsequent exposure to 520 nm (duration 10 s) causes the sheet to straighten again; (d) bending after exposure to 365 nm (10 s); (e) straightening after exposure to 520 nm (10 s). Scale bar = 50 μ m.

thickness (Supporting Information, Figure S12a,b). This layered rolled-up structure could also been seen in optical microscope images (Supporting Information, Figure S13). The number of times a microsheet rolled up on itself, defined as the $R^{\#}$, is given by $R^{\#} = L/(\pi D)$ where L is the length of the microsheet, and D is the diameter of the rolled cylinder produced. $R^{\#} = 7$ for the largest microsheets (Supporting Information, Figure S14).

After the initial exposure to visible light, the dramatic rolling and unrolling could not be repeated. We attempted to reset the sheets by exposing them to 365 nm light to promote the $Z \rightarrow E$ back reaction. The microsheets bent when exposed to 365 nm but did not roll up. This bend could be reversed by exposure to 520 nm light (Figure 6 and Movie S11). This P-type actuation could be cycled over 10 times, but additional irradiation cycles caused the microsheets to lose birefringence and eventually stop bending.

The initial rolling up under 520 nm light can be attributed to the formation of a layer of Z-ADUD at the sheet surface that generates a lattice contraction along the long axis of the crystal, perpendicular to the rolling up. 5,52,53 Powder X-ray diffraction experiments on microsheet samples deposited on an amorphous substrate did not yield identifiable peaks above the background, probably due to the ultrathin dimensions and small amount of sample. Without knowing the orientation of the crystal axes with respect to the microsheet dimensions, we were unable evaluate exactly how the $E \rightarrow Z$ isomerization contracts the crystal lattice. But we can surmise that the subsequent unrolling is caused by further conversion that more uniformly distributes the Z-isomer across the crystal thickness, reducing the stress due to the bimorph effect. The unrolled sheets are not completely converted to the Z isomer, however. HPLC analysis of the rolled and unrolled microsheets revealed that they had a similar 70:30 Z-ADUD/E-ADUD ratio as dry microsheets irradiated under the same conditions. The 70:30 ratio probably reflects the photostationary state achieved by 520 nm excitation of the E-**ADUD** in the solid state (Supporting Information, Figure S15). The dramatic initial rolling cannot be recovered because we never return to a situation where the Z and E isomers have the same anisotropic distribution across the crystal thickness necessary for high curvature bending. If a way could be found to cleanly switch between the E and Z forms in the crystal, then it should be possible to roll and unroll the sheets at will, limited only by mechanical fatigue of the crystal.

The unique behavior of *E*-ADUD is likely due to a combination of crystal packing and morphology factors, including

- a) The ability of the $E \rightarrow Z$ reaction to proceed in the metastable polymorph **B**.
- b) The ability to grow ultrathin sheets with low second moments that support high curvature bending.

- c) The resistance of these crystals to fracture despite their high curvature.
- d) The orientation of the $E \to Z$ contraction axis parallel to the long axis of the microsheets.

Previous workers have observed that clay,⁵⁴ gel^{55,56} and polymer sheets^{57,58} can be made to roll up into multilayer scrolls similar to those reported in this paper. However, those morphologies were static and could only be obtained under specific growth conditions, with no way to recover the flat sheet crystal. E-ADUD represents a system where both rolling and unrolling can be initiated by light. The cylindrical shape of the partially reacted crystal is similar to that observed for 9methylanthracene (9MA), where crystalline sheets suspended in water were observed to roll up and unroll with a similar radius of curvature.⁵³ One difference between the two systems is the ability to grow larger sheets of E-ADUD. The larger area of the E-ADUD sheets permits the formation of multilayer structures which effectively seal the edges of roll, leaving only the top and bottom ends open. A second difference is that in 9MA, the internal stress was created by a [4 + 4] photodimerization that can proceed to ~100% conversion because there is no photoproduct absorption at the excitation wavelength. When exposed to 365 nm, 9MA microsheets rolled and unrolled but were left as a static sheet after the photodimerization was completed throughout the crystal. Since there were no longer any molecules left to absorb the light, the fully photodimerized 9MA sheets were photochemically inert. E-ADUD, on the other hand, remains photochemically active even after unrolling and can be partially cycled using different excitation wavelengths.

CONCLUSIONS

Precipitation from an aqueous SDS/1-DD solution enabled the growth of highly crystalline microsheets composed of *E*-ADUD. These microsheets have submicron thicknesses and were composed of metastable crystal polymorph that enabled the E → Z photoisomerization to proceed. When exposed to visible light, the sheets rapidly rolled up into multilayered cylinders or scrolls. If the light was removed at this point, the microscrolls were stable indefinitely, but if it was turned on again, they unrolled back to their original flat shape. The unrolled microsheets retained some photomechanical activity by bending and unbending under alternating UV and visible light exposure. This dramatic photoinduced shape change could prove useful for applications like antenna or stent opening in hard-to-reach environments. The complex sequential shape changes originating from a single component crystal exemplify the complex photomechanical behavior that can arise when crystal polymorphism and morphology are controlled.

ASSOCIATED CONTENT

Supporting Information

The Supporting Information is available free of charge at https://pubs.acs.org/doi/10.1021/acs.cgd.4c00996.

¹H NMR spectra for all compounds, additional crystal data information, synthesis scheme, including images of experimental results (PDF)

Video of parallel cracks forming on the surface of the crystal (MP4)

Video of the curled *E*-ADUD microsheet (MP4)

Video of thicker microsheets developing minor cracks (MP4)

Video of sheets retaining their birefringence after unrolling (MP4)

Video of the behavior of the microsheets rolling up and unrolling in unison (MP4)

Second video of the behavior of the microsheets (MP4) Third video of the behavior of the microsheets (MP4) Fourth video of the behavior of the microsheets (MP4) Fifth video of the behavior of the microsheets (MP4) Sixth video of the behavior of the microsheets (MP4) Video of microsheets bending when exposed to 365 nm (MP4)

Accession Codes

CCDC 2371683—2371684 contain the supplementary crystallographic data for this paper. These data can be obtained free of charge via www.ccdc.cam.ac.uk/data_request/cif, or by emailing data_request/cif, or by contacting The Cambridge Crystallographic Data Centre, 12 Union Road, Cambridge CB2 1EZ, UK; fax: +44 1223 336033.

AUTHOR INFORMATION

Corresponding Authors

Christopher J. Bardeen — Department of Chemistry, University of California, Riverside, Riverside, California 92521, United States; orcid.org/0000-0002-5755-9476; Email: christopher.bardeen@ucr.edu

Rabih O. Al-Kaysi — College of Science and Health Professions-3124, King Saud bin Abdulaziz University for Health Sciences, King Abdullah International Medical Research Center, Ministry of National Guard Health Affairs, Riyadh 11426, Kingdom of Saudi Arabia; orcid.org/0000-0001-8429-2802; Email: rabihalkaysi@gmail.com, kaysir@ksauhs.edu.sa

Authors

Pranaya P. Ghate — Department of Chemical and Environmental Engineering, University of California, Riverside, Riverside, California 92521, United States

Cody J. Perry – Department of Chemistry, University of California, Riverside, Riverside, California 92521, United States

Veronica Carta — Department of Chemistry, University of California, Riverside, Riverside, California 92521, United States; ocid.org/0000-0001-8089-8436

Ibraheem Bushnak — College of Science and Health Professions-3124, King Saud bin Abdulaziz University for Health Sciences, King Abdullah International Medical Research Center, Ministry of National Guard Health Affairs, Riyadh 11426, Kingdom of Saudi Arabia

Yahya J. Almuallem — College of Science and Health Professions-3124, King Saud bin Abdulaziz University for Health Sciences, King Abdullah International Medical Research Center, Ministry of National Guard Health Affairs, Riyadh 11426, Kingdom of Saudi Arabia

Gregory J. O. Beran — Department of Chemistry, University of California, Riverside, Riverside, California 92521, United States; orcid.org/0000-0002-2229-2580

Complete contact information is available at: https://pubs.acs.org/10.1021/acs.cgd.4c00996

Notes

The authors declare no competing financial interest.

ACKNOWLEDGMENTS

This work was supported by the National Science Foundation, grant DMR-1810514 (C.J.B.), King Abdullah International Medical Research Center (KSAU-HS/KAIMRC) through grant NRC21R25003 (R.O.K) and CHE-1955554 (G.J.O.B.). Computer time to G.J.O.B. from ACCESS (CHE110064) is gratefully acknowledged.

REFERENCES

- (1) Kim, T.; Zhu, L.; Al-Kaysi, R. O.; Bardeen, C. J. Organic photomechanical materials. *ChemPhysChem* **2014**, *15*, 400–414.
- (2) White, T. J. Photomechanical Materials, Composites, and Systems: Wireless Transduction of Light into Work. 1 ed.; John Wiley & Sons: Hoboken, NJ, 2017.
- (3) Kuzyk, M. G.; Dawson, N. J. Photomechanical materials and applications: a tutorial. *Adv. Optics Photonics* **2020**, *12*, 847–1011.
- (4) Koshima, H. Mechanically Responsive Materials for Soft Robotics. 1 ed.; John Wiley & Sons: Weinheim, Germany, 2020.
- (5) Naumov, P.; Chizhik, S.; Panda, M. K.; Nath, N. K.; Boldyreva, E. Mechanically Responsive Molecular Crystals. *Chem. Rev.* **2015**, *115*, 12440–12490.
- (6) Awad, W. M.; Daniel, W.; Kitagawa, D.; Halabi, J. M.; Al-Handawi, M. B.; Tahir, I.; Tong, F.; Campillo-Alvarado, G.; Shtukenberg, A. G.; Alkhidir, T.; et al. Mechanical properties and peculiarities of molecular crystals. *Chem. Soc. Rev.* **2023**, *52*, 3098–3169.
- (7) Gao, L.; Hao, Y.; Zhang, X.; Huang, X.; Wang, T.; Hao, H. Polymorph induced diversity of photomechanical motions of molecular crystals. *CrystEngComm* **2020**, *22*, 3279–3286.
- (8) Jiang, Z.; Zhao, H.; Wu, W.; Chen, K.; Yu, H.; Wang, T.; Huang, X.; Wang, N.; Zhou, L.; Hao, H. Multi-stimuli responsive organic polymorphic crystals: anisotropic elasticity and plasticity, mechanochromism and photomechanical motions. *J. Mater. Chem. C* **2023**, *11*, 4375–4383
- (9) Gately, T. J.; Cook, C.; Almuzarie, R.; Islam, I.; Gardner, Z.; Iuliucci, R. J.; Al-Kaysi, R. O.; Beran, G. J. O.; Bardeen, C. J. Effect of Fluorination on the Polymorphism and Photomechanical Properties of Cinnamalmalononitrile Crystals. *Cryst. Growth. Des.* **2022**, 22, 7298–7307.
- (10) Koshima, H.; Ojima, N.; Uchimoto, H. Mechanical motion of azobenzene crystals upon photoirradiation. *J. Am. Chem. Soc.* **2009**, *131*, 6890–6891.
- (11) Morimoto, M.; Irie, M. A diarylethene cocrystal that converts light into mechanical work. *J. Am. Chem. Soc.* **2010**, 132, 14172–14178.
- (12) Bushuyev, O. S.; Tomberg, A.; Friscic, T.; Barrett, C. J. Shaping Crystals with Light: Crystal-to-Crystal Isomerization and Photomechanical Effect in Fluorinated Azobenzenes. *J. Am. Chem. Soc.* **2013**, *135*, 12556–12559.
- (13) Kitagawa, D.; Kobatake, S. Crystal Thickness Dependence of Photoinduced Crystal Bending of 1,2-Bis(2-methyl-5-(4-(1-naphthoyloxymethyl)phenyl)-3-thienyl)perfluorocyclopentene. *J. Phys. Chem. C* **2013**, *117*, 20887–20892.
- (14) Kitagawa, D.; Kobatake, S. Crystal thickness dependence of the photoinduced crystal bending of 1-(5-methyl-2-(4-(p-vinylbenzoylox-

- ymethyl)-phenyl)-4-thiazolyl)-2-(5-methyl-2-phenyl-4-thiazolyl)-perfluorocyclopentene. *Photochem. Photobiol. Sci.* **2014**, *13*, 764–769.
- (15) Kim, T.; Zhu, L.; Mueller, L. J.; Bardeen, C. J. Mechanism of Photoinduced Bending and Twisting in Crystalline Microneedles and Microribbons Composed of 9-Methylanthracene. *J. Am. Chem. Soc.* **2014**, *136*, 6617–6625.
- (16) Nath, N. K.; Pejov, L. o.; Nichols, S. M.; Hu, C.; Saleh, N. i.; Kahr, B.; Naumov, P. e. Model for Photoinduced Bending of Slender Molecular Crystals. *J. Am. Chem. Soc.* **2014**, *136*, 2757–2766.
- (17) Halabi, J. M.; Ahmed, E.; Sofela, S.; Naumov, P. Performance of molecular crystals in conversion of light to mechanical work. *Proc. Nat. Acad. Sci.* **2021**, *118*, No. e2020604118.
- (18) Al-Kaysi, R. O.; Muller, A. M.; Bardeen, C. J. Photochemically driven shape changes of crystalline organic nanorods. *J. Am. Chem. Soc.* **2006**, *128*, 15938–15939.
- (19) Ha, J.-M.; Wolf, J. H.; Hillmyer, M. A.; Ward, M. D. Polymorph Selectivity under Nanoscopic Confinement. J. Am. Chem. Soc. 2004, 126, 3382–3383.
- (20) Ha, J.-M.; Hamilton, B. D.; Hillmyer, M. A.; Ward, M. D. Phase Behavior and Polymorphism of Organic Crystals Confined within Nanoscale Chambers. *Cryst. Growth Des.* **2009**, *9*, 4766–4777.
- (21) Zhang, X.; Dong, C.; Zapien, J. A.; Ismathullakhan, S.; Kang, Z.; Jie, J.; Zhang, X.; Chang, J. C.; Lee, C.-S.; Lee, S.-T. Polyhedral Organic Microcrystals: From Cubes to Rhombic Dodecahedra. *Angew. Chem., Int. Ed.* **2009**, *48*, 9121–9123.
- (22) Lin, Z.-Q.; Sun, P.-J.; Tay, Y.-Y.; Liang, J.; Liu, Y.; Shi, N.-E.; Xie, L.-H.; Yi, M.-D.; Qian, Y.; Fan, Q.-L.; et al. Kinetically Controlled Assembly of a Spirocyclic Aromatic Hydrocarbon into Polyhedral Micro/Nanocrystals. *ACS Nano* **2012**, *6*, 5309–5319.
- (23) Al-Kaysi, R. O.; Zhu, L.; Al-Haidar, M.; Al-Muhannah, M. K.; El-Boubbou, K.; Hamdan, T. M.; Bardeen, C. J. Chemical reaction method for growing photomechanical organic microcrystals. *CrystEngComm* **2015**, *17*, 8835–8842.
- (24) Yang, S.-H.; Lin, Z.-Q.; Shi, N.-E.; Jin, L.-Z.; Yu, M.-N.; Xie, L.-H.; Yia, M.-D.; Huang, W. A Polyhedral Supramolecular System of Endocyclic Crystalline Organic Nanostructures: the Case of Triptycenes. *CrystEngComm* **2015**, *17*, 1448–1452.
- (25) Peng, L.; Chen, Y.-N.; Dong, Y. Q.; He, C.; Wang, H. Surfactant-Assisted Self-Assembled Polymorphs of AIEgen Di(4-propoxyphenyl)-dibenzofulvene. *J. Mater. Chem. C* **2017**, *5*, 557–565.
- (26) Park, Y.; Koo, J. Y.; Choi, H. C. Additive-Free Morphology Control of Organic Polyhedral Molecular Crystals by the Antisolvent Molecular Geometry: From Rod, Disk, to Cube. *Cryst. Growth Des.* **2018**, *18*, 7239–7243.
- (27) Xu, T.-Y.; Tong, F.; Xu, H.; Wang, M.-Q.; Tian, H.; Qu, D.-H. Engineering Photomechanical Molecular Crystals to Achieve Extraordinary Expansion Based on Solid-State [2 + 2] Photocycloaddition. *J. Am. Chem. Soc.* **2022**, 144, 6278–6290.
- (28) Tong, F.; Al-Haidar, M.; Zhu, L.; Al-Kaysi, R. O.; Bardeen, C. J. Photoinduced peeling of molecular crystals. *Chem. Commun.* **2019**, *55*, 3709–3712.
- (29) Tong, F.; Kitagawa, D.; Bushnak, I.; Al-Kaysi, R. O.; Bardeen, C. J. Light-Powered Autonomous Flagella-Like Motion of Molecular Crystal Microwires. *Angew. Chem., Int. Ed.* **2021**, *60*, 2414–2423.
- (30) Sheldrick, G. M. A short history of SHELX. *Acta Cryst. A* **2008**, 64, 112–122.
- (31) Sheldrick, G. M. SHELXT Integrated space-group and crystalstructure determination. *Acta Cryst. A* **2015**, *71*, 3–8.
- (32) Dolomanov, O. V.; Bourhis, L. J.; Gildea, R. J.; Howard, J. A. K.; Puschmann, H. OLEX2: a complete structure solution, refinement and analysis program. *J. Appl. Crystallogr.* **2009**, *42*, 339–341.
- (33) Shi, D.; Nannenga, B. L.; Iadanza, M. G.; Gonen, T. Three-dimensional electron crystallography of protein microcrystals. *eLife* **2013**, 2, No. e01345.
- (34) Giannozzi, P.; Andreussi, O.; Brumme, T.; Bunau, O.; Nardelli, M. B.; Calandra, M.; Car, R.; Cavazzoni, C.; Ceresoli, D.; Cococcioni, M.; et al. Advanced capabilities for materials modelling with Quantum ESPRESSO. *J. Phys.: Condens. Matter* **2017**, *29*, 465901.

- (35) Becke, A. D. On the large-gradient behavior of the density functional exchange energy. *J. Chem. Phys.* **1986**, *85*, 7184–7187.
- (36) Perdew, J. P.; Burke, K.; Ernzerhof, M. Generalized Gradient Approximation Made Simple. *Phys. Rev. Lett.* **1996**, *77*, 3865–3868.
- (37) Otero-de-la-Roza, A.; Johnson, E. R. Van der Waals interactions in solids using the exchange-hole dipole moment model. *J. Chem. Phys.* **2012**, *136*, 174109.
- (38) Greenwell, C.; Beran, G. J. O. Inaccurate Conformational Energies Still Hinder Crystal Structure Prediction in Flexible Organic Molecules. *Cryst. Growth Des.* **2020**, *20*, 4875–4881.
- (39) Neese, F. The ORCA program system. *WIREs Comp. Mol. Sci.* **2012**, 2, 73–78.
- (40) Jiang, H.; Zhang, J.-M.; Du, W.-Q.; Zhu, S.-Z. A Convenient Synthesis of Novel Meldrum's Acid C_{60} Fullerene Derivatives. *Chin. J. Chem.* **2007**, 25, 86–89.
- (41) Tong, F.; Chen, S.; Li, Z.; Liu, M.; Al-Kaysi, R. O.; Mohideen, U.; Yin, Y.; Bardeen, C. J. Crystal-to-Gel Transformation Stimulated by a Solid-State EZ Photoisomerization. *Angew. Chem., Int. Ed.* **2019**, *58*, 15429–15434.
- (42) Ramamurthy, V.; Venkatesan, K. Photochemical reactions of organic crystals. *Chem. Rev.* **1987**, *87*, 433–481.
- (43) Gately, T. J.; Sontising, W.; Easley, C. J.; Islam, I.; Al-Kaysi, R. O.; Beran, G. J. O.; Bardeen, C. J. Effect of halogen substitution on energies and dynamics of reversible photomechanical crystals based on 9-anthracenecarboxylic acid. *CrystEngComm* **2021**, *23*, 5931–5943.
- (44) Garti, N.; Zour, H. The effect of surfactants on the crystallization and polymorphic transformation of glutamic acid. *J. Cryst. Growth* **1997**, 172, 486–498.
- (45) Davey, R. J.; Dowling, R. J.; Cruz-Cabeza, A. J. The Impact of Ionic Surfactants on the Crystallisation of Glycine Polymorphs. *Isr. J. Chem.* **2021**, *61*, 573–582.
- (46) Penha, F. M.; Gopalan, A.; Meijlink, J. C.; Ibis, F.; Eral, H. B. Selective Crystallization of d-Mannitol Polymorphs Using Surfactant Self-Assembly. *Cryst. Growth Des.* **2021**, *21*, 3928–3935.
- (47) Semjonova, A.; Bērziņš, A. Surfactant Provided Control of Crystallization Polymorphic Outcome and Stabilization of Metastable Polymorphs of 2,6-Dimethoxyphenylboronic Acid. *Crystals* **2022**, *12*, 1738
- (48) Nangia, A. Conformational Polymorphism in Organic Crystals. *Acc. Chem. Res.* **2008**, *41*, 595–604.
- (49) Andrade, E. N. d. C.; Randall, R. F. Y.; Makin, M. J. The Rehbinder Effect. *Proc. Phys. Soc. B* **1950**, *63*, 990–995.
- (50) Malkin, A. I. Regularities and mechanisms of the Rehbinder's effect. *Colloid J.* **2012**, *74*, 223–238.
- (51) Xu, T.-Y.; Cui, M.; Zhao, C.; Zhou, S.-W.; Zhang, T.-L.; Lin, H.-Y.; Tong, F.; Qu, D.-H. Visible Light-Induced Collapse of Molecular Microcrystals into Droplets by E-to-Z Photoisomerization and Melting Phase Transition. *CCS Chem.* **2024**, *6*, 1071–1084.
- (52) Chen, Z.; Majidi, C.; Srolovitz, D. J.; Haataja, M. Tunable Helical Ribbons. *Appl. Phys. Lett.* **2011**, *98*, No. 011906.
- (53) Tong, F.; Xu, W.; Al-Haidar, M.; Kitagawa, D.; Al-Kaysi, R. O.; Bardeen, C. J. Photomechanically Induced Magnetic Field Response by Controlling Molecular Orientation in 9-Methylanthracene Microcrystals. *Angew. Chem., Int. Ed.* **2018**, *57*, 7080–7084.
- (54) Lvov, Y.; Wang, W.; Zhang, L.; Fakhrullin, R. Halloysite Clay Nanotubes for Loading and Sustained Release of Functional Compounds. *Adv. Mater.* **2016**, *28*, 1227–1250.
- (55) Takahashi, M.; Figus, C.; Malfatti, L.; Tokuda, Y.; Yamamoto, K.; Yoko, T.; Kitanaga, T.; Tokudome, Y.; Innocenzi, P. Strain-driven self-rolling of hybrid organic—inorganic microrolls: interfaces with self-assembled particles. *NPG Asia Mater.* **2012**, *4*, No. e22.
- (56) Liang, S.; Chen, Q.; Huang, X.; Yang, B.; Guo, Y.; Naumov, P.; Zhang, L. Conversion of flat to cylindrical hydrogel structures by asymmetric crosslinking and ionic exchange. *Chem. Eng. J.* **2024**, *490*, No. 151906.
- (57) Peng, L.; Zhu, J.; Agarwal, S. Self-Rolled Porous Hollow Tubes Made up of Biodegradable Polymers. *Macromol. Rapid Commun.* **2017**, 38, 1700034.

(58) Teshima, T. F.; Nakashima, H.; Ueno, Y.; Sasaki, S.; Henderson, C. S.; Tsukada, S. Cell Assembly in Self-foldable Multilayered Soft Micro-rolls. *Sci. Rep.* **2017**, *7*, 17376.